High variability in organic carbon sources and microbial activities in the hadopelagic waters

Xinxin Li [1]*, Xin Zhao,[1] Hongyue Dang,[2]* Chuanlun Zhang,[1] Igor Fernández-Urruzola [3] Zhiqiang Liu,[1] Frank Wenzhöfer,[4,5,6] Ronnie N. Glud[6,7,8]

[1]Department of Ocean Science and Engineering, Southern University of Science and Technology, Shenzhen, China
[2]State Key Laboratory of Marine Environmental Science, Fujian Key Laboratory of Marine Carbon Sequestration, College of Ocean and Earth Sciences, Xiamen University, Xiamen, China
[3]Millennium Institute of Oceanography, University of Concepción, Concepción, Chile
[4]HGF-MPG Group for Deep Sea Ecology & and Technology, Alfred Wegener Institute Helmholtz Centre for Polar and Marine Research, Bremerhaven, Germany
[5]Max Planck Institute for Marine Microbiology, Bremen, Germany
[6]Department of Biology, University of Southern Denmark, Odense M, Denmark
[7]Tokyo University of Marine Science and Technology, Tokyo, Japan
[8]Danish Institute for Advanced Study-DIAS, University of Southern Denmark, Odense, Denmark

Abstract

Hadal sediments are recognized as organic carbon depocenters with intensified microbial activity compared to adjacent abyssal sites due to focusing of relatively labile organic materials. However, the sources and turnover of hadopelagic organic carbon and its linkages to microbial activities have not been studied. We present the first synergic research on particulate organic carbon, dark carbon fixation, and size-fractionated microbial community respiration proxy over the Atacama Trench. The results demonstrate that all parameters attenuate rapidly from surface to mesopelagic water (∼ 1000 m). Progressing deeper, values remain relatively stable throughout bathypelagic (∼ 4000 m) and abyssopelagic (∼ 6000 m) waters. However, in the hadopelagic zone (> 6000 m), highly variable values indicate dynamic organic carbon sources and microbial activities in the deepest trench. On average, 71% of the microbial community respiration proxy is attributable to particle-associated communities, indicating importance of particles for microbial metabolism. No apparent relationship was observed between the microbial community respiration proxy and microbial 16S rRNA gene abundance below the epipelagic depth, indicating variable supply and quality of organic carbon likely constrained heterotrophic activities rather than microbial abundances in the deep ocean. The depth-integrated dark carbon fixation (> 1000 m) accounts for 11.5% ± 7.6% of the surface net primary production, of which 2.9% ± 0.4% is from hadopelagic depth. Dark carbon fixation is thus an important in situ organic carbon source for hadal life. This study suggests that high variability in organic carbon sources and microbial activities in the hadopelagic trench cannot be simply extrapolated from findings in the shallower dark ocean (e.g., 1000–6000 m).

*Correspondence: lixinxin@sustech.edu.cn; danghy@xmu.edu.cn

Hadal trenches cover less than 2% of the global ocean. However, they include 45% of the oceanic depth range that covers the epipelagic (0–200 m), mesopelagic (200–1000 m), bathypelagic (1000–4000 m), abyssopelagic (4000–6000 m), and hadopelagic (> 6000 m) realms (Schrope 2014). Their V-shaped bathymetry, unique hydrographical conditions, high seismic activity, extreme hydrostatic pressure, and biogeographical isolation distinguish the hadopelagic environment from the other pelagic layers (Jamieson 2015). Recent work has documented intensified microbial activity in hadal sediments compared to adjacent abyssal sites (Glud et al. 2013). This is presumably facilitated by enhanced deposition and diagenesis of nutritious organic carbon along the

trench axis due to downslope sediment transport triggered by frequent earthquake activities (Turnewitsch et al. 2014; Turner 2015) that is linked to both bend-faulting (Ranero et al. 2003; Morgan and Ranero 2023) of the incoming plate and the forearc's seismic activity (Sippl et al. 2018). However, little is known about the linkages between organic carbon cycling and microbial activities in extreme depths.

One enigma in pelagic water is the apparent imbalance between the biological pump-mediated particulate organic carbon (POC) supply rate and the microbial organic carbon consumption rate in the dark global ocean (Burd et al. 2010). Even the highest estimates of sinking POC flux determined by sediment traps would only explain about half of the measured respiratory oxygen consumption in the dark ocean on a global average (del Giorgio and Duarte 2002). Suspended (i.e., non-sinking) POC may reduce such an imbalance (Arístegui et al. 2009; Baltar et al. 2010). Physical processes such as lateral transport (Shen et al. 2020), nepheloid layers (Chronis et al. 2000), and turbidity flows (Paull et al. 2018), especially downslope the V-shaped trench sides could also introduce extra POC. In addition, in situ dark carbon fixation can help to balance the dark ocean's carbon budget. For example, about 12–72% of the microbial community carbon demand in the mesopelagic Atlantic Ocean is potentially supplied by in situ dark carbon fixation (Baltar et al. 2010). Dark carbon fixation has also been shown to contribute significantly to heterotrophic carbon demand in the mesopelagic northeast Atlantic (Baltar et al. 2016), the bathypelagic Atlantic waters off the Galician coast (Guerrero-Feijóo et al. 2018), the deep Mediterranean Sea (Celussi et al. 2017), the mid and lower water column of the upwelling regions in the Arabian Sea (Lengger et al. 2019), the tropical South China Sea (Zhou et al. 2017), and the deep-sea sediments of the Mediterranean Sea and the northeastern Atlantic Ocean (Molari et al. 2013). However, the quantitative contribution of dark carbon fixation to the hadopelagic organic carbon budget remains unmeasured to date.

Microbial community respiration plays a critical role in determining the microbial organic carbon consumption rate and vertical carbon transport in the ocean (Packard et al. 2015). However, quantification of the microbial community respiration from the deep ocean is sparse (del Giorgio and Duarte 2002). Highly sensitive methods based on in vivo or in vitro respiratory electron transport system activity have thus been developed as a proxy for microbial community respiration (Martinez-Garcia et al. 2009).

Although they are likely to define the key factors that determine deep-sea organic carbon dynamics (Nagata et al. 2010; Middelburg 2011; Herndl and Reinthaler 2013), the POC, dark carbon fixation, and microbial community respiration have not been measured simultaneously in hadopelagic waters. Here we conduct a synergic investigation of POC, dark carbon fixation, and size-fractionated microbial community respiration proxy over the full water depths of the Atacama Trench.

Our results are then related to the net primary production (NPP) in the surface ocean and the microbial gene copy numbers in each sample. This approach leads to new insights into the sources and microbial metabolisms of organic carbon in hadopelagic waters.

Methods

Site description and sample collection

Located at an intense upwelling region with an average primary production of ~ 270 g C m^{-2} yr^{-1}, the Atacama Trench ranks among one of the most productive marine ecosystems encountered above any hadal realm (Jamieson et al. 2010). During a 30-d cruise on RV SONNE (SO261) in March 2018, water samples targeting selected depths across the epipelagic to hadopelagic zones were collected from five sites (A2, A3, A4, A5, and A6) along the Atacama Trench axis and at an oceanward abyssal reference site (A7; Fig. 1; Supporting Information Table S1). A rosette water sampler equipped with 24 ten-liter Niskin bottles and standard Conductivity, Temperature, Depth (CTD) sensors (Sea-Bird Scientific) for conductivity, temperature, and depth measurement was used to collect water samples at predefined depths. Standard CTD profiles were resolved to a depth of 6000 m. A custom-built autonomous rosette sampler containing six Niskin bottles (8 or 12 liters each) was used to sample the hadopelagic waters. Each bottle was closed at a preprogrammed water depth triggered by a pressure sensor.

The NPP was calculated using the standard Vertically Generalized Production Model (Behrenfeld and Falkowski 1997). Estimates of annual (2003–2018) average NPP over each site were calculated using the standard Vertically Generalized Production Model (Behrenfeld and Falkowski 1997) and remote sensing data (NASA Goddard Space Flight Center, Ocean Ecology Laboratory, Ocean Biology Processing Group. Moderate-resolution Imaging Spectroradiometer [MODIS] Aqua Chlorophyll Data; 2018 Reprocessing; NASA OB.DAAC, Greenbelt, MD, USA. doi:10.5067/AQUA/MODIS/L3M/CHL/2018.).

The detailed information for the sampling sites and annual average surface water NPP are listed in Table 1 and Supporting Information Figure S1.

Particulate organic carbon sampling and analysis

Water samples were obtained at several depths between 5 and 8000 m for the analysis of POC at sites A2, A4, and A6 (Supporting Information Table S1). Sixty liters of seawater were first prefiltered through 20 μm and then filtered onto precombusted (450°C, 24 h) Whatman GF/F filters (47 mm ø, nominal pore size 0.7 μm) for each sample. Filters with particles were dried at 60°C for 24 h, then wrapped in precombusted aluminum foil and stored in a sealed container with silica gel. Before analysis, filters were placed overnight in a desiccator saturated with HCl fumes to remove any
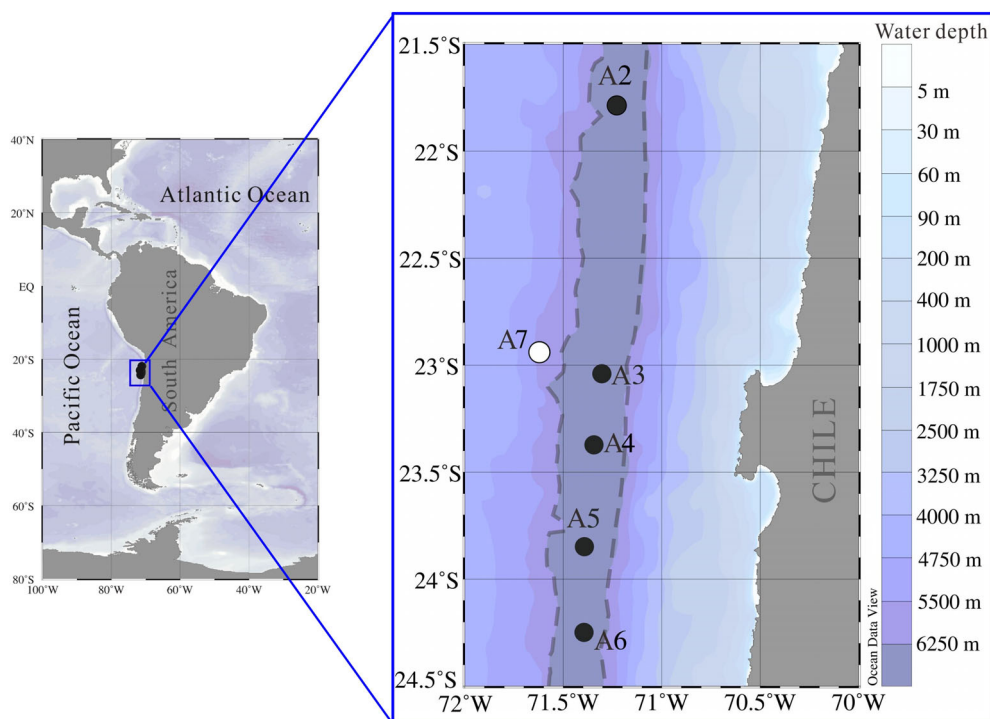
Fig. 1. Sampling sites in this study along the Atacama Trench during SO261 cruise by RV SONNE in March, 2018. A7 is used as the abyssal reference site while the other sites are along the trench axis which is enclosed by the dashed black line.

Table 1. Detailed information for the sampling sites in the Atacama Trench, along with annual average NPP.

Parameters	Reference site	Hadal sites (from north to south)				
	A7	A2	A3	A4	A5	A6
Latitude (°S)	22.94	21.78	23.05	23.36	23.82	24.27
Longitude (°W)	71.62	71.21	71.30	71.34	71.37	71.42
Maximum water depth (m)	5500	7994	7915	8085	7770	7720
NPP (mg C m^{-2} d^{-1})	828	837	911	928	924	878

carbonate and then moved into a new desiccator with silica gel. Dried filters were subsequently packed into tin capsules and then fed into an elemental analyzer (Thermo Scientific Flash 2000 CHN EA; Universidad de Concepción) for POC concentration (mg m^{-3}) analysis in the Laboratory of Biogeochemistry and Applied Stable Isotopes, Pontifical Catholic University of Chile. The analytical error of the filter blank is lower than 3 μg which corresponds to 0.03–0.8% of the measured values.

Dark carbon fixation rate measurement

The dark carbon fixation rate experiment was conducted at sites A2, A4, and A6 (Supporting Information Table S1) according to the procedure of Hama et al. (1983). Briefly, seawater samples from each depth were transferred into precombusted 1-liter glass bottles and spiked with 10 mL of 20 mM NaH^{13}CO$_3$ solution (99 atom% ^{13}C, Cambridge Isotope Laboratories) with a final

concentration of about 10% of the total ambient inorganic carbon (Kwak et al. 2013). Then, the samples were incubated in darkness at in situ temperature for 120 h. Immediately after incubation, samples were filtered directly through precombusted (450°C for 4 h) Whatman GF/F filters (47 mm ø, ~ 0.7 μm pore size) under a gentle vacuum. The filters were kept frozen and stored at −80°C until further isotopic analysis.

After freeze-drying, the filters were cut in half and treated with concentrated HCl vapors (12 N) for 6 h. The filters were then packed in tin capsules in a 48-well tray and analyzed at the UC Davis Stable Isotope Facility, using a PDZ Europa ANCA-GSL elemental analyzer interfaced to a PDZ Europa 20–20 isotope ratio mass spectrometer (Sercon Ltd.). The final isotope results are expressed in δ notation (‰) relative to international standards Vienna PeeDee Belemnite. The standard deviation for quadruplicate analysis was always within 0.46‰ of the sample values.

The volume-specific dark carbon fixation rate (μg C m^{-3} d^{-1}) is obtained using the following equation (Hama et al. [1983](); Mousseau et al. [1995]()):

$$\text{Dark carbon fixation rate} = \frac{C(a_{is} - a_{ns})}{t(a_{ic} - a_{ns})} \times 1000$$

where a_{is} is the atom% of ^{13}C in the incubated sample; a_{ns} is the atom% of ^{13}C in the natural sample; a_{ic} is the atom% of ^{13}C in the total inorganic carbon (i.e., ^{13}C added/[^{13}C added + dissolved inorganic carbon]); C is the POC in the incubated sample (mg C m^{-3}); and t is the incubation time in days.

Microbial community respiration proxy measurement

The enzymatic electron transport system drives oxidative phosphorylation. It has frequently been used as a proxy for respiration (Minutoli and Guglielmo [2009](); Villegas-Mendoza et al. [2019]()). In vivo electron transport system activity was measured at in situ temperature based on tetrazolium salt 2-para(iodo-phenyl)-3(nitrophenyl)-5(phenyl)tetrazolium chloride (INT) reduction rate following the protocol of Martinez-Garcia et al. ([2009]()). Briefly, two control replicates of 500 mL of seawater collected from each water depth of all sites were immediately fixed with formaldehyde (2% w/v final concentration) for 15 min. Then 12.5 mL of 7.9 mM INT solution was added to each of the killed-controls and the triplicate seawater samples (500 mL each; final INT concentration of 0.2 mM) to incubate for 1 h. The incubated samples were then fixed with formaldehyde for 15 min before being sequentially filtered through polycarbonate filters (47 mm Whatman) as suggested by Martinez-Garcia et al. ([2009]()); Martinez-Garcia et al. ([2018]()). The sizes of 3.0, 0.8, and 0.2 μm pore size were chosen to best match the sizes for the microbial gene abundance analysis described below. The filters were then stored in cryovials at $-80°$C until their further analysis for the amount of formazan (INT-F) produced from INT reduction. No prefiltration was carried out for sampled seawater. Therefore, the INT reduction rates may include the activity of small zooplankton in addition to the activity of microplankton that mainly includes the prokaryotes (bacteria and archaea), nano flagellates, and ciliates for the samples retained on the 3.0 μm pore-size filters (>3.0 μm). A pretest was conducted that showed linear INT-F accumulation rates during the relevant incubation period.

For further analysis, 1 mL of propanol was added to each cryovial containing the INT-F filters, followed by its sonication (47 kHz) in 50°C water baths for 30 min and vertexing for 1–2 min. Next, propanol extract containing INT-F was transferred to a 1.5-mL microcentrifuge tube and centrifuged at 13,200g, 18°C for 10 min. The absorbance of the supernatant was measured at 485 nm using a UV-VIS Spectrophotometer (UV-2600, Shimadzu). A standard curve constructed using 12 different concentrations (ranging from 0.02 to 42 μM, dissolved in propanol) of pure INT-F was used to calibrate the concentrations of sample INT-F. Considering the potential uncertainties in the conversion ratio between microbial community respiration and electron transport system activity under different oceanic conditions (Arístegui et al. [2003](); Reinthaler et al. [2006](); García-Martín et al. [2019]()), the in vivo INT reduction rate in the unit of mmol m^{-3} d^{-1} used as a proxy for potential electron transport system activity was applied as the microbial community respiration proxy. In addition, the microbial community respiration proxy of the > 0.8 and 0.2–0.8 μm size fractions were separately calculated to assess the relative contributions of the particle-associated and free-living microbial subcommunities to the total microbial community respiration proxy, respectively.

Microbial quantitative polymerase chain reaction (qPCR) analysis

Seawater samples (2–9.75 liters) from different water depths at sites A2, A4, and A6 (Supporting Information Table S1) were collected on-deck and successively filtered through GF/F filters with pore sizes of 2.7 μm (Whatman), 0.7 μm (Whatman), and 0.3 μm (Advantec, Japan) and stored at $-80°$C until further analyses. Microbial community genomic DNA was extracted from the filter samples in the laboratory using the DNeasy Power Soil Kit (QIAGEN) according to the manufacturer's instructions. Archaeal and bacterial 16S rRNA gene abundances were determined using SYBR Green qPCR assays with primer sets 787F (ATTAGATACCCSBGTAGTCC)/915R (GTGCTCCCCCGCCAAT TCCT) and 338F (ACTCCTACGGGAGGCAG)/805R (GACTACCA GGGTATCTAA TCC), respectively (Thijs et al. [2017]()).

The qPCR solution contained 1 μL template DNA, 5 μL SYBR Premix Ex Taq^{TM}II (TaKaRa Biotechnology Co.), 0.4 μL each primer, 0.2 μL ROX Reference DyeII (TaKaRa Biotechnology Co.), and 3 μL deionized water. The qPCR conditions were as follows: initial denaturation at 95°C for 30 s, followed by 40 cycles of denaturation at 95°C for 5 s, annealing at 55°C for 45 s, and extension at 72°C for 1 min. Each sample was measured in triplicate. The amplification efficiency of bacterial and archaeal 16S rRNA genes was about 95% and 85%, respectively. The microbial 16S rRNA gene abundance in the unit of copies mL^{-1} was calculated as the sum of bacterial and archaeal 16S rRNA gene abundance and was used as a proxy for the microbial abundance. In addition, the gene abundances of the > 0.7 and 0.3–0.7 μm size fractions were separately calculated to assess the relative contributions of the particle-associated and free-living microbial subcommunities to the total prokaryotic community abundance, respectively.

Data regression analysis

The depth attenuation of the analyzed parameters is expressed by the normalized power function as defined by Martin et al. ([1987]()):

$$R = R_{100} \times \left(\frac{z}{100}\right)^b$$

where R is the parameter (e.g., POC, microbial community respiration proxy, or gene copy numbers) analyzed at any specific depth; z is the depth in meters; and R_{100} is the modeled parameter value at 100 m depth, where Atacama Trench surface water photosynthesis usually ceases due to light limitation (Fernández-Urruzola et al. 2021).

A plot of $\log R$ vs. $\log(z/100)$ would give an intercept that yields the value of $\log R_{100}$ and a slope that yields the value of the exponent b, the absolute value of which is the flux attenuation coefficient. Statistically significant differences were identified using a one-way ANOVA at a 95% confidence interval ($p < 0.05$).

Results

The POC concentrations and dark carbon fixation rates

The concentration of POC declines from 129.0 mg C m^{-3} (A2, 20 m), 115.8 mg C m^{-3} (A4, 20 m), and 95.7 mg C m^{-3} (A6, 5 m) in the epipelagic zone to 16.3 mg C m^{-3} (A2, 1000 m), 14.0 mg C m^{-3} (A4, 1000 m), and 13.3 mg C m^{-3} (A6, 1000 m) in the mesopelagic zone (Fig. 2A; Table 2), respectively. Thereafter, values remain relatively uniform until 6000 m, with a single excursion for A6 at 5000 m. In hadopelagic waters, values tend to increase and become more variable in comparison with those in the abyssopelagic zone, in particular at A2 and A4. Although the POC concentration typically follows the normalized power function at all sites above 6000 m ($R^2 > 0.94$, $p < 0.05$, Table 2), the hadal data points overshoot each regression line of the power function at

A2 and A4 (Fig. 2A). The attenuation coefficient for POC concentration from the surface to 6000 m ranges from 0.35 (A4, A6, $p < 0.05$) to 0.38 (A2, $p < 0.05$; Fig. 2A; Table 3).

Dark carbon fixation rates were resolved at a coarser resolution. These range from 4.3 to 561.7 μg C m^{-3} d^{-1} (Fig. 2B; Table 2). The profiles generally exhibit similar depth patterns as the POC concentration patterns, that is, a distinct decline from the epipelagic to the mesopelagic zone, and thereafter remaining relatively constant throughout the abyssopelagic zone. At hadopelagic depths, however, the dark carbon fixation rates exhibit highly variable patterns. For example, the dark carbon fixation rate increases to 19.6 ± 3.5 μg C m^{-3} d^{-1} (7000 m) at A2, which is 3.9 times higher than the average rate of dark carbon fixation between 1000 and 6000 m (5.1 ± 0.6 μg C m^{-3} d^{-1}). In contrast, A6 shows a decreasing trend (Fig. 2B).

Quantitatively, the whole water depth-integrated dark carbon fixation rates (248.3–368.0 mg C m^{-2} d^{-1}) are equivalent to 31.2% ± 3.6% (A2), 39.7% ± 17.4% (A4), and 28.3% ± 4.6% (A6) of the annual average NPP of the euphonic zone, or an average of 33.0% ± 13.0% for the three sites (Table 2). For waters below 1000 m, the depth-integrated dark carbon fixation rates (50.0–175.0 mg C m^{-2} d^{-1}) are equivalent to 6.0% ± 2.0% (A2), 8.7% ± 3.3% (A4), and 19.9% ± 4.5% (A6) of the annual average NPP, or an average of 11.5% ± 7.6% for the three sites (Table 2), in which 2.9% ± 0.4% is from the hadopelagic depth, indicating the importance of the dark carbon fixation in the deep ocean.

Size-fractionated microbial community respiration proxy

At the abyssal site A7, the microbial community respiration proxy of the three size fractions decreases sharply by 59% (0.2–0.8 μm), 75% (0.8–3.0 μm), and 87% (> 3.0 μm) from the epipelagic to mesopelagic zone (1000 m), and then stays at relatively low and constant levels down to 5000 m (Supporting Information Table S2). The numbers for the > 3.0 μm fraction drop from 22.0 ± 0.9 mmol m^{-3} d^{-1} ($n = 3$) at 5 m depth to 2.8 ± 0.6 mmol m^{-3} d^{-1} ($n = 3$) at 1000 m, and then maintain an average of 3.1 ± 0.3 mmol m^{-3} d^{-1} ($n = 9$) between 1000 and 5000 m. This general pattern is apparent at all sites overlying hadal water depths (Fig. 3; Supporting Information Table S2). The values of particle-associated microbial community respiration proxy also decrease significantly, by 58% (A6) to 93% (A2), from the epipelagic to the mesopelagic zone (1000 m) at all sites (average of 76.4% ± 13.4%; Fig. 3; Table 3) and have no significant depth variations between 1000 and 5000 m while ranging from 9.7 ± 0.9 mmol m^{-3} d^{-1} at A2 to 87.2 ± 0.1 mmol m^{-3} d^{-1} at A3 (Table 3).

In the hadopelagic zone, however, the depth profiles of microbial community respiration proxy clearly exhibit higher variability. For instance, at A2, the microbial community respiration proxy for 0.8–3.0 μm fraction increases significantly from 8.3 ± 1.2 mmol m^{-3} d^{-1} at 6000–7000 m ($n = 9$) to 167.3 ± 102.1 mmol m^{-3} d^{-1} at 7500 m ($n = 3$), nearly the
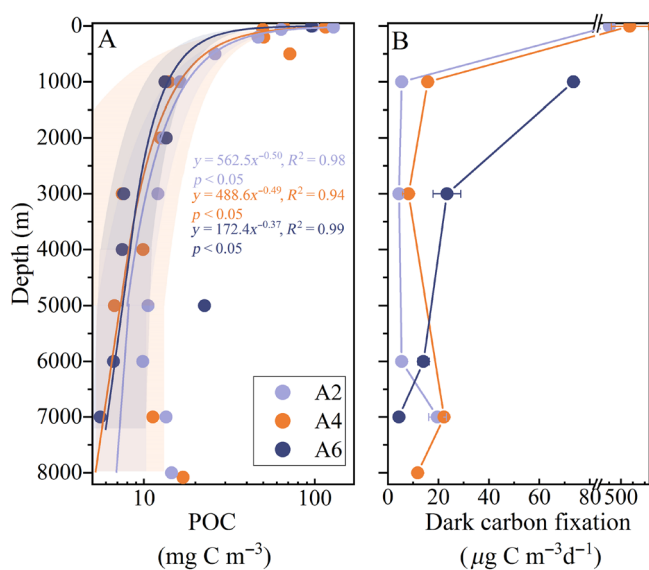
Fig. 2. Depth profiles of (**A**) POC (log scale), and (**B**) dark carbon fixation rates at sites A2, A4, and A6. The shadow in (**A**) shows 95% confidence intervals for the normalized power function regression of POC.

Table 2. The POC, dark carbon fixation rates (DCF), depth-integrated dark carbon fixation rates (mg C m^{-2} d^{-1}), and their comparison with annual average NPP (%) in the study area. The numbers in parenthesis in the last column indicate the percentage for 0–6000 m depth integration.

Sites	Depth (m)	POC (mg m^{-3})	Dark carbon fixation rates (μg C m^{-3} d^{-1})	Depth-integrated dark carbon fixation rate (mg C m^{-2} d^{-1})	DCF/NPP (%)
A2	5	97.5	418.7 ± 12.1		31.2 ± 3.6 (28.1 ± 3.1)
	20	129.0	—		
	60	63.6	—		
	200	46.5	—		
	500	26.1	—		
	1000	16.3	5.5 ± 1.3	211.0 ± 9.4 (5–1000 m)	
	2000	13.0	—		
	3000	12.1	4.3 ± 1.9		
	4000	7.5	—		
	5000	10.6	—		
	6000	9.9	5.4 ± 0.3	24.5 ± 8.9 (1000–6000 m)	
	7000	13.5	19.6 ± 3.5	12.5 ± 2.6 (6000–7000 m)	
	8000	14.5	—	12.9 (7000–8000 m)*	
A4	5	65.6	561.7 ± 130.4		39.7 ± 17.4 (36.4 ± 17.1)
	20	115.8	—		
	60	49.8	—		
	200	50.3	—		
	500	71.5	—		
	1000	14.0	15.8 ± 1.1	287.3 ± 92.5 (0–1000 m)	
	2000	12.5	—		
	3000	7.5	8.1 ± 1.4		
	4000	9.9	—		
	5000	6.7	—	50.7 ± 19.4 (1000–6000 m)	
	7000	11.3	22.2 ± 1.5	12.94 (6000–7000 m)*	
	7000	12.0	—		
	8000	16.9	11.8 ± 1.7	17.1 ± 2.2 (7000–8000 m)	
A6	5	95.7	—		28.3 ± 4.6 (25.8 ± 4.2)
	1000	13.3	73.4 ± 1.0	73.4 ± 0.7 (0–1000 m)†	
	2000	13.5	—		
	3000	7.6	23.3 ± 5.5		
	4000	7.5	—		
	5000	22.6	—		
	6000	6.6	14.0 ± 2.3	152.8 ± 25.5 (1000–6000 m)	
	7000	5.6	4.4 ± 1.1	9.2 ± 2.4 (6000–7000 m)	
	8000	—	—	12.9 (7000–8000 m)*	

Dashes (—) indicate no sampling.
*Estimated using the mean value of the 1000 m integrated number in hadal zone.
†Integrated DCF of A6 was an underestimation because of the lack of data at 5 m.

same magnitude of change as that encountered in the epipelagic layer. This trend was also seen in the other two size fractions (Fig. 3; Supporting Information Table S2). A different pattern was observed at A3: the microbial community respiration proxy of > 3.0 and 0.8–3.0 μm fractions decreases from the abyssopelagic to the deepest sampling depth, but the microbial community respiration proxy of 0.2–0.8 μm fraction is similar to the values of the overlying water (Fig. 3; Supporting Information Table S2). The higher variability of the depth profiles in the hadopelagic water is also apparent for the particle-associated microbial community respiration proxy (Fig. 3; Supporting Information Table S2). The particle-associated fractions either increase significantly with depth (82%, 7500 m) in comparison with overlying water (53% ±

Table 3. Summary of the particle-associated (PA) and free-living (FL) fractions of microbial community respiration proxy (MCRP), the PA fraction (PA, %), and the parameters for their normalized power function at each site. MCRP with depths are expressed using the normalized power function, MCRP = MCRP$_{100}$ × (z/100)^b, where MCRP is the INT reduction rate at any depth up to 6000 m, MCRP$_{100}$ is the MCRP at 100 m depth (the log-log intercept), z is the depth in meters, and the exponent, b, is the log-log slope, n is the number of replicates of each depth. The number in parenthesis indicates the standard deviation for three replicate incubations.

Site ID		A2			A3			A4			A5			A6			A7		
Layer	Depth (m)	PA	FL	PA (%)	PA	FL	PA (%)	PA	FL	PA (%)	PA	FL	PA (%)	PA	FL	PA (%)	PA	FL	PA (%)
Microbial community respiration proxy																			
Epipelagic	5	131.8 (19.3)	51.2 (2.9)	72.0 (10.7)	230.7 (18.1)	23.4 (3.5)	90.8 (8.7)	198.9 (19.5)	80.2 (22.6)	71.3 (8.4)	275.0 (13.7)	44.9 (1.2)	86.0 (4.4)	116.3 (42.0)	28.1 (4.4)	76.9 (17.8)	68.3 (2.1)	11.9 (1.9)	85.1 (3.1)
Mesopelagic	1000	9.7 (0.9)	9.6 (0.5)	50.1 (3.9)	87.2 (6.3)	14.5 (2.5)	85.7 (8.1)	36.5 (4.6)	34.6 (5.2)	51.4 (7.8)	41.9 (5.9)	26.6 (5.6)	61.2 (8.7)	48.5 (13.7)	20.2 (3.8)	70.6 (20.2)	14.3 (2.1)	4.9 (0.7)	74.4 (11.0)
Bathypelagic	3000	10.0 (1.3)	9.0 (0.4)	52.8 (5.5)	87.1 (20.5)	12.6 (1.2)	88.5 (3.9)	35.5 (6.6)	24.9 (8.2)	58.8 (12.3)	38.6 (15.6)	25.2 (6.1)	64.4 (13.2)	59.9 (10.8)	16.4 (6.1)	77.2 (14.2)	14.1 (1.1)	4.2 (0.5)	77.1 (6.1)
Abyssopelagic	6000	10.1 (0.8)	7.6 (1.3)	57.1 (5.8)	91.8 (12.2)	13.9 (1.2)	86.9 (11.1)	37.7 (2.6)	23.7 (5.4)	61.4 (7.0)	47.7 (7.2)	21.7 (3.9)	68.8 (12.3)	41.3 (14.5)	19.7 (9.9)	67.7 (28.7)	15.1 (2.0)*	3.9 (0.8)*	79.4 (10.1)
Hadopelagic	6500	10.5 (3.1)	6.7 (0.7)	60.9 (15.7)	—	—	—	—			—	—		28.3 (10.5)	30.1 (10.3)	51.3 (15.5)	—	—	
	7000	11.4 (2.1)	7.6 (1.5)	60.0 (10.6)	—			50.0 (17.4)	23.8 (8.7)	67.7 (25.4)	108.8 (14.1)	12.3 (2.2)	89.9 (11.3)	35.7 (5.1)	35.6 (4.7)	50.1 (6.7)	—		
	7500	176.7 (103.1)	41.4 (16.6)	82.3 (11.7)	50.4 (10.9)	13.0 (1.8)	79.4 (21.1)	49.3 (4.5)†	21.8 (0.9)†	69.3 (5.7)	49.2 (4.4)	19.9 (6.8)	71.2 (10.0)	46.2 (8.1)	18.0 (6.0)	70.3 (12.3)	—		
	8000	—			—			49.5 (8.0)	30.7 (11.6)	61.7 (12.4)	—			—			—		
Mean‡		66.2 (95.7)	18.6 (6.3)	67.8 (12.7)	50.4 (10.9)	13.0 (1.8)	79.4 (21.1)	49.6 (0.4)	25.4 (7.1)	66.2 (14.5)	79.0 (42.2)	16.1 (4.5)	80.5 (10.7)	36.7 (9.0)	27.9 (7.0)	57.2 (11.5)	—		
Normalized power function parameters																			
Total microbial community respiration proxy	b	-0.23			-0.16			-0.19			-0.19			-0.16			-0.25		
	R$_{100}$	68.8			158.1			143.4			157.5			120.7			43.8		
	R^2	0.27			0.88			0.87			0.73			0.86			0.92		
	n	3			3			3			3			3			3		
POC§	b	-0.38			—			-0.35			—			-0.35			—		
	R$_{100}$	47.0			—			43.6			—			33.3			—		
	R^2	0.92			—			0.73			—			0.79			—		

*Sampling depth of 5000 m.
†Sampling depth of 7700 m.
‡Mean MCRP of hadopelagic.
§0.7-μm filter for POC analysis.
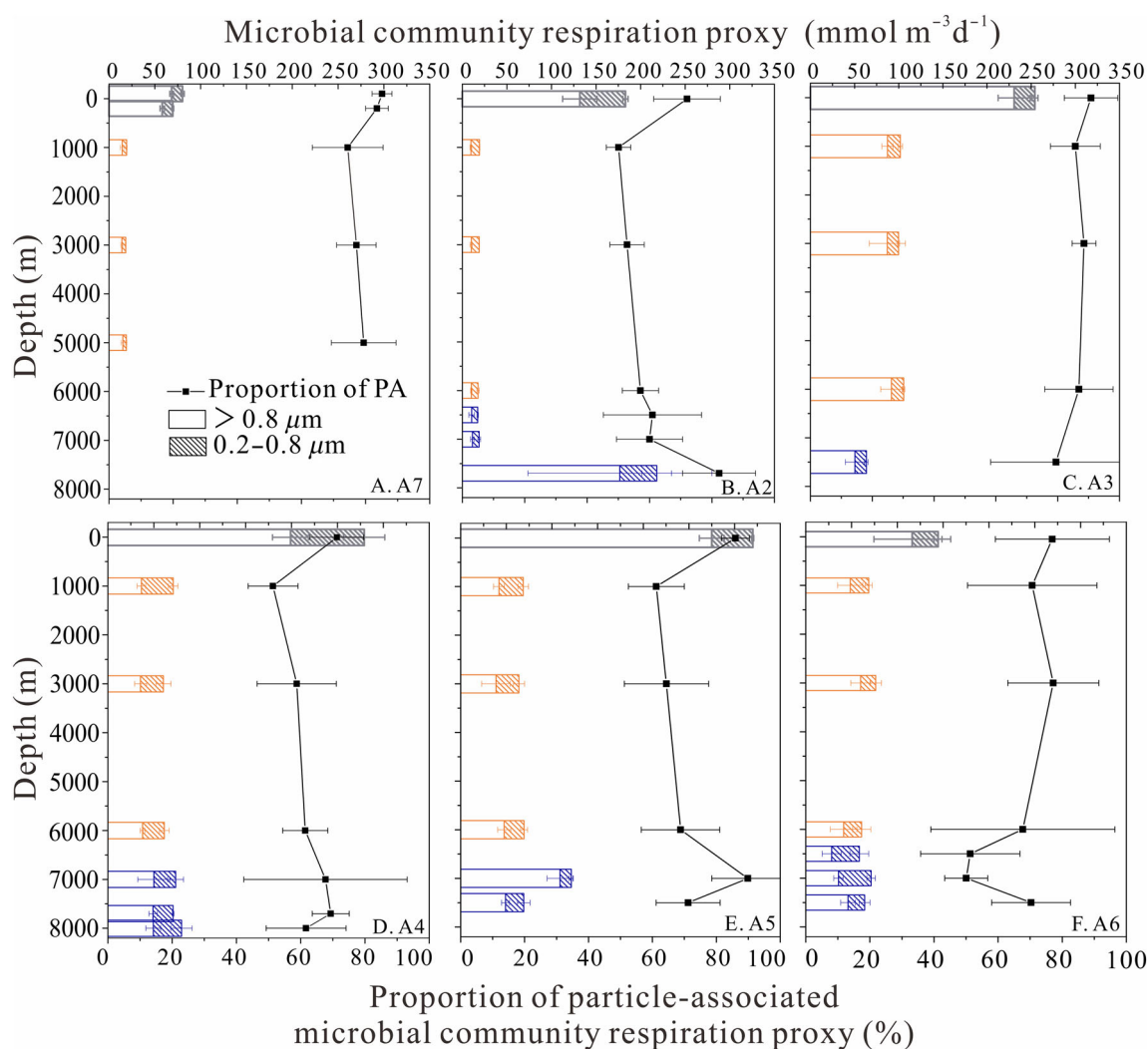
Fig. 3. The microbial community respiration proxy (mmol m^{-3} d^{-1}) in particle-associated (PA, > 0.8 μm, or sum of the 0.8–3.0 and > 3.0 μm fractions) and free-living (0.2–0.8 μm) fractions in the sampling sites of Atacama Trench. Bars of gray, orange, and dark blue represented the epipelagic, dark ocean, and hadopelagic zone, respectively. The black dotted line indicated the proportion of particle-associated microbial community respiration proxy at each site.

3.5%, 1000–6000 m) at A2, or decrease with depth as seen as at A3. Enhanced variability is also reflected in the relatively high standard deviation of microbial community respiration proxy within each sample in the hadal depth, and considerable variation between respective sites. There is either a maximum peak of microbial community respiration proxy (A4 and A5) or a minimum value (A6) in the hadopelagic water between 6000 m and the deepest sampling depth (Fig. 3).

Normalized power functions from the surface to 6000 m were fitted to the total microbial community respiration proxy (Table 3). The patterns seen in these regression lines closely follow those of POC with an attenuation coefficient ranging from 0.16 (A6, $p < 0.01$) to 0.25 (A7, $p < 0.01$;

Table 3). Similarly, the microbial community respiration proxy in the hadopelagic layer deviates from the extrapolated regression lines reflecting higher variability among sites in the hadopelagic waters (e.g., Fig. 3C vs. Fig. 3B,E). Measurements exceeded the fitted curve at A2, A4, and A5 and are comparable at A6, while measurements at A3 are lower than the optimized curve fit.

The microbial gene copy numbers

The mid-sized fraction of 0.7–2.7 μm shows the highest microbial gene copy numbers among the three fractions at the three targeted hadal sites (Supporting Information Table S3). Vertically, the total values are generally higher in the epipelagic layer than those between 1000 and 6000 m at each site
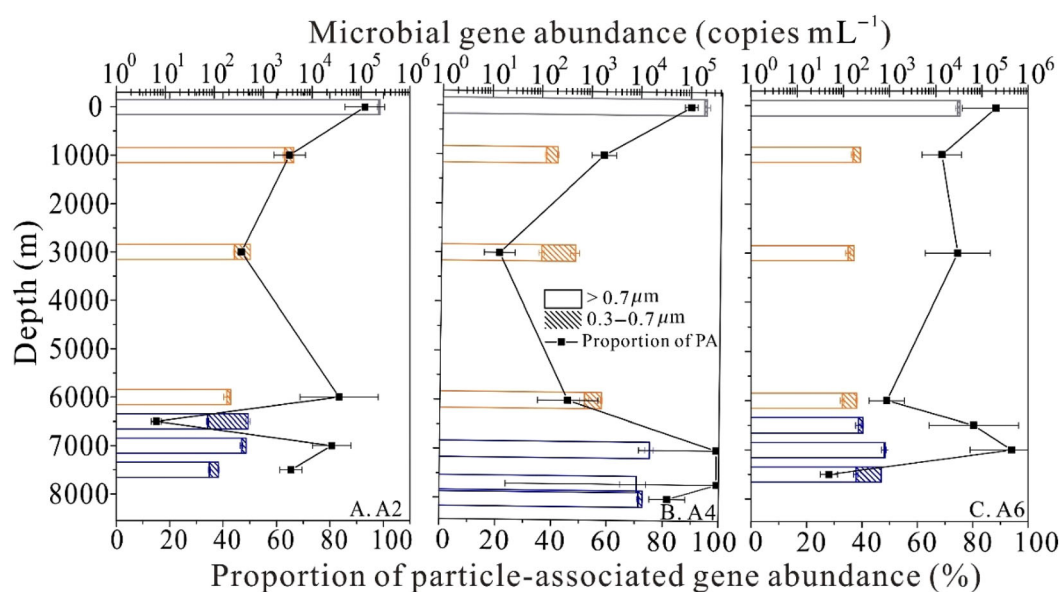
Fig. 4. The log scale of microbial gene abundance on particle-associated (PA, > 0.7 μm, or sum of 0.7–2.7 and > 2.7 μm fractions) and free-living (0.3–0.7 μm) microbial community (copies mL^{-1}) based on 16s rRNA analysis at selected sites of (**A**) A2, (**B**) A4, and (**C**) A6 in the Atacama Trench. Bars of light blue, orange, and dark blue represented epipelagic, dark ocean, and hadopelagic zone, respectively. The black dotted line indicated the % proportion of the particle-associated gene abundance at each site.

Table 4. Summary of the gene copy numbers for particle-associated (PA) and free-living (FL) fractions, the proportion of PA fraction (PA, %), and the parameters for their normalized power function at each site.

Site ID		A2			A4			A6		
Gene copy numbers (copies mL^{-1})										
Layer	Depth (m)	PA	FL	PA (%)	PA	FL	PA (%)	PA	FL	PA (%)
Epipelagic	5	2.3×10^5	1.7×10^4	93.1	1.9×10^5	2.3×10^4	89.0	3.0×10^4	3.9×10^3	88.4
		(1.3×10^4)	(3.4×10^2)	(7.4)	(3.0×10^3)	(1.0×10^3)	(2.2)	(2.9×10^3)	(4.3×10^2)	(12.2)
Mesopelagic	1000	2.7×10^3	1.5×10^3	64.9	1.2×10^2	8.9×10	57.9	1.6×10^2	7.2×10	68.9
		(1.9×10^2)	(5.1×10)	(5.9)	(6.5)	(5.0)	(4.4)	(1.1×10)	(6.5)	(7.2)
Bathypelagic	3000	2.6×10^2	2.9×10^2	46.9	1.0×10^2	4.0×10^2	20.8	1.3×10^2	4.3×10	74.7
		(5.6)	(3.4)	(1.3)	(1.3×10)	(1.0×10^2)	(5.5)	(1.5×10)	(3.5)	(11.7)
Abyssopelagic	6000	1.8×10^2	3.6×10	83.4	8.2×10^2	9.8×10^2	45.7	9.5×10	9.9×10	49.0
		(2.4×10)	(1.7)	(14.6)	(1.7×10^2)	(5.7×10)	(10.8)	(8.7)	(9.1)	(6.4)
Hadopelagic	6500	7.4×10	4.2×10^2	15.0	—	—	—	2.1×10^2	5.2×10	80.4
		(4.1)	(4.9×10)	(1.8)				(3.1×10)	(7.2)	(16.2)
	7000	3.6×10^2	8.7×10	80.7	1.7×10^4	1.6×10^2	99.1	7.6×10^2	4.8×10	94
		(2.2×10)	(7.1)	(7.2)	(3.4×10^3)	(1.1×10)	(27.8)	(8.6×10)	(3.0)	(14.9)
	7500	8.0×10	4.2×10	65.5	9.4×10^3	7.0×10	99.3	1.9×10^2	4.7×10^2	28.1
		(2.8)	(3.6)	(4.2)	(5.1×10^3)	(1.2×10)	(75.6)	(1.9×10)	(1.1×10)	(3.10)
	8000	—	—		1.0×10^4	2.3×10^3	81.7			—
					(5.2×10^2)	(2.3×10^2)	(6.4)			
	Mean*	1.7×10^2	1.8×10^2	48.5	1.2×10^4	8.4×10^2	93.6	3.8×10^2	1.9×10^2	66.8
		(1.6×10^2)	(2.0×10)	(4.9)	(4.2×10^3)	(6.0×10)	(31.8)	(3.2×10^2)	(7)	(9.9)

*Mean gene copy numbers of hadopelagic.

(Fig. 4; Supporting Information Table S3). Variation patterns in size-fractionated gene copy numbers between 1000 and 6000 m (Fig. 4) do not follow the patterns of the POC and microbial community respiration proxy profiles.

The hadopelagic layer, again, shows enhanced variations at all sites. There is either a maximum (e.g., 0.7–2.7 μm fraction at A2) or minima (e.g., 0.3–0.7 μm fraction at A4) in the microbial gene abundance in comparison with the values in the bathypelagic or abyssopelagic depth ranges (Supporting Information Table S3).

Apart from a few exceptions, the gene copy numbers of the particle-associated fraction are generally higher than the free-living fraction. On average, the particle-associated fraction amounts to 68% $\pm$ 25% of the total gene copy numbers (Fig. 4; Table 4).

Discussion

The hadopelagic realm has been largely unexplored, so that very little is known about its carbon and energy flows. Although this study spanned a limited time interval, the resolved POC turnover in the deep pelagic realm cannot be directly linked to its relatively uniform ancillary data of temperature and salinity (Fernández-Urruzola et al. 2021) and concurrent NPP (Supporting Information Fig. S1). The results also provide surprising insights into the transport and variability of organic carbon based on multiple hadal sites. They reinforce the increasing realization that the biogeochemical and microbial functions of the geologically unique hadopelagic zone cannot be understood by simply extrapolating findings from shallower deep ocean depths.

POC availability in the Atacama Trench

It has been reported that sinking POC fluxes generally decline following a power law with depth (Martin et al. 1987), while non-sinking POC usually do not follow the normalized power function (Baltar et al. 2010). Although the filtration process and the well-fit depth profiles of POC concentration at the three hadal sites prevent a clear distinction between sinking vs. non-sinking POC, it is meaningful to compare the attenuation coefficients of POC in this study to those of the POC flux to indicate their degradation ability with depths. The attenuation coefficients (0.35–0.38; Fig. 2A; Table 3) found are similar to but lower than average global attenuation coefficients for POC flux (0.64–0.86; Henson et al. 2012; Gloege et al. 2017). Generally, the attenuation coefficients of POC fluxes are relatively high in the oligotrophic ocean, as at the central Pacific subtropical station ALOHA (Buesseler et al. 2007), subtropical gyre sites in the Northwest Pacific (Honda 2020) and North Atlantic (0.70–1.59, Berelson 2001), and in the open Pacific Ocean (Martin et al. 1987; Supporting Information Table S4). In contrast, relatively low POC attenuation coefficients are generally associated with productive waters, for example, the PERU station off Peru (0.32, Martin

et al. 1987), in subtropical regions (0.3–0.5 with a minimum of 0.24, Henson et al. 2012), and in the Australia–Indonesia coastal province (0.42, Guidi et al. 2015). This is thought to be linked to fast-sinking POC such as diatom aggregates and zooplankton fecal pellets in the highly productive Chilean coast (Jamieson et al. 2010) which may contribute importantly to sinking/non-sinking POC and their fluxes (González et al. 2009; Eduardo Menschel and González 2019; Fernández-Urruzola et al. 2021).

In fact, many surface ocean-originated fast-sinking biogenic particles can reach the deep water and hadal sediments in relatively fresh conditions (Danovaro et al. 2003; Glud et al. 2021). For example, it has been found that there are significant inputs of surface ocean-derived organic carbon with younger radiocarbon ages to the sediments of the Atacama Trench (Xu et al. 2021). In addition, it has been recently reported that the degradation of hadal-pressure-exposed fast-sinking POC could be partially or entirely inhibited (Stief et al. 2021). This could protect the sinking-labile POC from degradation. Extensive intermediate oxygen-depleted waters in this region may also slow down POC remineralization and facilitate efficient labile POC flux to the Atacama Trench (Fernández-Urruzola et al. 2021). More importantly, the V-shaped trench mostly traps these complex sources of labile organic carbon which can lead to highly elevated benthic organic carbon remineralization along the trench axis in comparison with that in adjacent abyssal sediments.

Of the three sites with water column POC concentrations, two sites (A2 and A4) show higher POC concentrations in the hadopelagic waters than in their overlaying abyssopelagic waters (Fig. 2A). The deep increases could be due to pulse input of photosynthesized POC with time lags from higher net primary production at the surface (Supporting Information Fig. S1), but more importantly, this indicates extra organic carbon inputs besides the sinking POC in the hadopelagic environments. Lateral transport of sediment and POC frequently occur in the eastern boundary regions with coastal upwelling (Lovecchio et al. 2017). This will be further enhanced by turbidity current, near-bottom gravity flow, and seismically induced sediment instabilities. In a deep-sea trench, there will be topography facilitated material transport along the steep trench sides into the hadal environments. For instance, sediment trap samples collected at 8500–8800 m in the Japan Trench showed more abundant POC than the sediment trap samples collected at shallower depths (Ishiwatari et al. 2000). Therefore, hadopelagic waters can harbor an elevated or highly variable abundance of POC in comparison with their overlying water masses (e.g., A2 and A4, Fig. 2).

The current study also identifies microbial dark carbon fixation to be an important source of autochthonous organic carbon in the hadopelagic waters and above (Fig. 2B). On the one hand, volume-specific dark carbon fixation rates in the Atacama Trench are similar in magnitude to those in most other open oceans (0.1–547.2 μg C m^{-3} d^{-1}), but they are one or

two magnitudes lower than in coastal and other energy-rich waters (e.g., 5.5–35 mg C m^{-3} d^{-1}; Supporting Information Table S5). On the other hand, our results suggest that above 6000 m, the ratio of depth-integrated dark carbon fixation to annual euphotic NPP is 30% $\pm$ 12% (Table 2), which is significantly higher than the globally estimated ratio of ca. 2%. (Middelburg 2011) or as much as 25% in some specific deep-sea settings (Follett et al. 2014; Guerrero-Feijóo et al. 2018). The ratio is estimated to be 2.9% $\pm$ 0.4% for hadopelagic depths, also significantly higher than the traditional estimate of $\sim$ 1% NPP that could reach the seafloor through sedimentation (Sigman and Hain 2012). The ratio in this study may not have a high enough error as we did not consider the potential biases related to pore sizes, variabilities in NPP, and so on. Nevertheless, the results underline the potential importance of in situ chemosynthetic activity for the supply of newly fixed carbon and the sustenance of hadal life.

Noting that the current study represents a snapshot in time and that the dark carbon fixation rates measured under surface pressure may differ from in situ values, our results can be used to estimate dark carbon fixation rates with bias. For instance, the filtration step during the dark carbon fixation experiment excluded most free-living microorganisms such as the marine ammonia-oxidizing archaea, a group of chemolithotrophs that are widely distributed in hadal trenches (Nunoura et al. 2015, 2016). Therefore, our current assessment probably represented a minimum estimate for dark carbon fixation. Meanwhile, the pressure tolerance of the deep-sea microorganisms has yet to be clearly quantified (Amano et al. 2022), so that the atmospheric pressure used here could have a positive or negative effect on the dark carbon fixation assay. In any case, our experimental results presented the first evidence of the importance of in situ dark carbon fixation as a biogenic carbon source that directly contributes to elevated POC concentrations in the hadopelagic Atacama Trench (Fig. 2).

POC turnover in the pelagic realm: insight from microbial community respiration proxy

In the epipelagic water, the microbial community respiration proxy at 1000 m (R_{100}) correlates significantly with surface NPP ($R^2 = 0.93$, $p = 0.001$, Fig. 5A), which indicates that POC turnover is affected by the available POC introduced from NPP. Meanwhile, the microbial community respiration proxy is also significantly correlated with the microbial 16S rRNA gene abundance in the Atacama Trench (Fig. 5B). Therefore, the abundance of microbial communities is significant when determining their microbial respiration proxy, hence their ability to turnover POC.

In waters between 1000 and 6000 m, microbial community respiration proxy is relatively uniform, and 1–3 orders of magnitudes lower than those of the epipelagic water at each sampling site (Fig. 3). This finding is in agreement with the widely acknowledged conclusion that the maximum sinking POC turnover usually occurs in the mesopelagic zone (Martin
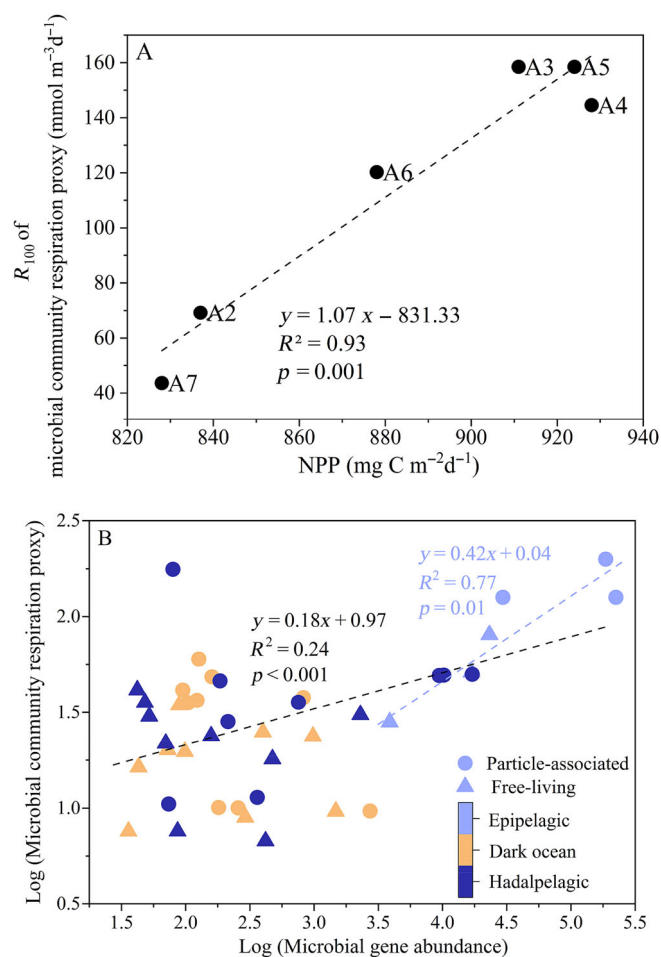
Fig. 5. (**A**) The annual average NPP vs. microbial community respiration proxy at 100 m depth (R_{100}) derived from the normal power regression. (**B**) Logarithmic scale of the particle-associated (> 0.8 μm) and free-living microbial community respiration proxy (0.2–0.8 μm; mmol m^{-3} d^{-1}) vs. gene abundance (> 0.7 and 0.3–0.7 μm, copies mL^{-1}) at sites A2, A4, and A6 in the Atacama Trench. Dotted lines in light blue and black represent the linear fits of the epipelagic layer and all the data, respectively.

et al. 1987), but is usually uniform in the general dark ocean such as in the water columns of the NE Pacific Ocean (Druffel et al. 1998), the Arctic Ocean (Griffith et al. 2012), the Sulu Sea (Ferrera et al. 2018), the Eastern Fram Strait (Engel et al. 2019), and so on. The attenuation coefficients of the vertical profiles of microbial community respiration proxy are significantly lower (0.16–0.23) than the corresponding coefficients of the vertical POC profiles (0.35–0.38, Table 3), indicating high levels of microbial community respiration at the corresponding depths. The microbial community respiration proxy is decoupled from the microbial 16S rRNA gene abundance below the epipelagic depth ($R^2 = 0.24$, $p < 0.001$, Fig. 5B), suggesting that the microbial community respiration depends mainly on the availability of organic matter (i.e., its quantity and quality as respiratory substrates) rather than on

the microbial abundance in the seawater above the Atacama Trench.

In the hadopelagic Atacama Trench, the highly variable vertical patterns of microbial community respiration proxy among sites are linked with the variable sources of respiratory organic substrates for microbial activities. The microbial community respiration proxy is also decoupled from the microbial 16S rRNA gene abundance (Fig. 5B). Although it is still unclear whether there are unique (Liu et al. 2019) or uniform (Tian et al. 2018) bacteria communities in the hadal zone, some heterotrophic deep sea-enriched bacteria in these studies indicate that elevated microbial activity may occur in the hadal environment. Particles containing labile organic carbon further stimulated microbial activities in Atacama Trench (Fig. 3, Fernández-Urruzola et al. 2021). The predominant contribution of particle-associated microbial community respiration proxy (69% ± 12% [$n = 54$, 1000–6000 m] and 70% ± 10% [$n = 36$, > 6000 m]; Table 3) and particle-associated microbial gene abundance compared to those of the free-living microbial fractions (Figs. 3, 4; Supporting Information Table S3) indicate locally enhanced microbial activities on POC, so that marine organic particles are hotspots for microbial heterotrophy and inorganic nutrient regeneration. This in turn provides nutrients and energy substrates that promote dark carbon fixation (Arnosti 2011; Herndl and Reinthaler 2013) that contribute as much as 25% of organic carbon in the deep ocean (Follett et al. 2014; Guerrero-Feijóo et al. 2018). Indeed, chemolithoautotrophic microbes such as ammonia-oxidizing archaea have been frequently detected in the Mariana Trench (Nunoura et al. 2015, 2016; Tarn et al. 2016). Ammonia-oxidizing archaea secrete organic compounds that may fuel microbial heterotrophy in the ocean (Bayer et al. 2019). A recent publication based on bacterial and eukaryotic intact polar lipids showed the importance of bacterial in situ production as a key source of labile organic matter in the Atacama Trench surface sediments (Flores et al. 2022). Our current study discovered that the increased dark carbon fixation activities in some of the hadopelagic waters of the Atacama Trench (e.g., site A2 and possibly site A4, Fig. 2B) can potentially provide an important source of freshly made organic carbon that contributes to alleviating the elevated carbon demand in these extreme environments (Figs. 2, 4). Direct comparisons showed that the dark carbon fixation (> 0.7 μm) is insignificantly correlated with the particle-associated microbial community respiration proxy ($R^2 = 0.91$, $p = 0.17$) and significantly correlated with particle-associated microbial gene copy numbers significantly ($R^2 = 0.92$, $p = 0.07$) in the hadalpelagic Atacama Trench, further supporting the idea that dark carbon fixation is an important POC source that feeds microbial communities and their respiration within the trench.

Summary

This study provides a first–step approach to explore the supply and microbial turnover of POC in the hadopelagic

Atacama Trench. Although previous studies have suggested a potential linkage between surface dynamics and deep-sea ecosystem processes in the region, the results shown here demonstrate that hadal settings exhibit high variability in the distribution of POC and microbial community respiration proxies, variations that presumably reflect complex and intense deposition dynamics and mass flows in the trench interior. In addition, the results suggest that enhanced chemosynthetic inputs may contribute significantly to pelagic productivity in sustaining life at hadal depths.

The current study relies on incubation at atmospheric pressure in order to assay deep-sea microbial activities. Future investigations which employ microbial incubations that are maintained or reestablished at in situ pressure conditions have the potential to obtain better results about microbial in situ activities in the hadopelagic extreme environments.

Data availability statement

The authors declare that all data and references supporting the findings of this study are included within the paper.

References

Amano, C., and others. 2022. Impact of hydrostatic pressure on organic carbon cycling of the deep-sea microbiome. bioRxiv: 2022.03.31.486587. doi:10.1101/2022.03.31.486587

Arístegui, J., S. Agustí, and C. M. Duarte. 2003. Respiration in the dark ocean. Geophys. Res. Lett. **30**: 1041. doi:10.1029/2002GL016227

Arístegui, J., J. M. Gasol, C. M. Duarte, and G. J. Herndld. 2009. Microbial oceanography of the dark ocean's pelagic realm. Limnol. Oceanogr. **54**: 1501–1529. doi:10.4319/lo.2009.54.5.1501

Arnosti, C. 2011. Microbial extracellular enzymes and the marine carbon cycle. Annu. Rev. Mar. Sci. **3**: 401–425. doi:10.1146/annurev-marine-120709-142731

Baltar, F., J. Aristegui, E. Sintes, J. M. Gasol, T. Reinthaler, and G. J. Herndl. 2010. Significance of non-sinking particulate organic carbon and dark CO_2 fixation to heterotrophic carbon demand in the mesopelagic northeast Atlantic. Geophys. Res. Lett. **37**: L09602. doi:10.1029/2010gl043105

Baltar, F., D. Lundin, J. Palovaara, I. Lekunberri, T. Reinthaler, G. J. Herndl, and J. Pinhassi. 2016. Prokaryotic responses to ammonium and organic carbon reveal alternative CO_2 fixation pathways and importance of alkaline phosphatase in the mesopelagic North Atlantic. Front. Microbiol. **7**: 1670. doi:10.3389/fmicb.2016.01670

Bayer, B., R. L. Hansman, M. J. Bittner, B. E. Noriega-Ortega, J. Niggemann, T. Dittmar, and G. J. Herndl. 2019. Ammonia-oxidizing archaea release a suite of organic compounds potentially fueling prokaryotic heterotrophy in the ocean. Environ. Microbiol. **21**: 4062–4075. doi:10.1111/1462-2920.14755

Behrenfeld, M. J., and P. G. Falkowski. 1997. Photosynthetic rates derived from satellite-based chlorophyll concentration. Limnol. Oceanogr. **42**: 1–20. doi:10.4319/lo.1997.42.1.0001

Berelson, W. M. 2001. The flux of particulate organic carbon into the ocean interior: A comparison of four U.S. JGOFS Regional Studies. Oceanography **14**: 59–67. doi:10.5670/oceanog.2001.07

Buesseler, K. O., and others. 2007. Revisiting carbon flux through the ocean's twilight zone. Science **316**: 567–570. doi:10.1126/science.1137959

Burd, A. B., and others. 2010. Assessing the apparent imbalance between geochemical and biochemical indicators of meso- and bathypelagic biological activity: What the @$♯! is wrong with present calculations of carbon budgets? Deep-Sea Res. II Top. Stud. Oceanogr. **57**: 1557–1571. doi:10.1016/j.dsr2.2010.02.022

Celussi, M., F. Malfatti, P. Ziveri, M. Giani, and P. Del Negro. 2017. Uptake-release dynamics of the inorganic and organic carbon pool mediated by planktonic prokaryotes in the deep Mediterranean Sea. Environ. Microbiol. **19**: 1163–1175. doi:10.1111/1462-2920.13641

Chronis, G., V. Lykousis, D. Georgopoulos, V. Zervakis, S. Stavrakakis, and S. Poulos. 2000. Suspended particulate matter and nepheloid layers over the southern margin of the Cretan Sea (N.E. Mediterranean): seasonal distribution and dynamics. Prog. Oceanogr. **46**: 163–185. doi:10.1016/S0079-6611(00)00017-3

Danovaro, R., N. Della Croce, A. Dell'Anno, and A. Pusceddu. 2003. A depocenter of organic matter at 7800 m depth in the SE Pacific Ocean. Deep-Sea Res. I Oceanogr. Res. Pap. **50**: 1411–1420. doi:10.1016/j.dsr.2003.07.001

del Giorgio, P. A., and C. M. Duarte. 2002. Respiration in the open ocean. Nature **420**: 379–384. doi:10.1038/nature01165

Druffel, E. R. M., S. Griffin, J. E. Bauer, D. M. Wolgast, and X.-C. Wang. 1998. Distribution of particulate organic carbon and radiocarbon in the water column from the upper slope to the abyssal NE Pacific Ocean. Deep-Sea Res. II Top. Stud. Oceanogr. **45**: 667–687. doi:10.1016/s0967-0645(98)00002-2

Eduardo Menschel, A., and H. E. González. 2019. Carbon and calcium carbonate export driven by appendicularian faecal pellets in the Humboldt Current System off Chile. Sci. Rep. **9**: 16501. doi:10.1038/s41598-019-52469-y

Engel, A., and others. 2019. Inter-annual variability of organic carbon concentration in the eastern fram strait during summer (2009–2017). Front. Mar. Sci. **6**: 187. doi:10.3389/fmars.2019.00187

Fernández-Urruzola, I., O. Ulloa, R. N. Glud, M. H. Pinkerton, W. Schneider, F. Wenzhöfer, and R. Escribano. 2021. Plankton respiration in the Atacama Trench region: Implications for particulate organic carbon flux into the hadal realm. Limnol. Oceanogr. **66**: 3134–3148. doi:10.1002/lno.11866

Ferrera, C. M., G. S. Jacinto, C.-T. A. Chen, and H.-K. Lui. 2018. Organic carbon concentrations in high- and low-productivity areas of the Sulu Sea. Sustainability **10**: 1867. doi:10.3390/su10061867

Flores, E., S. I. Cantarero, P. Ruiz-Fernández, N. Dildar, M. Zabel, O. Ulloa, and J. Sepúlveda. 2022. Bacterial and eukaryotic intact polar lipids point to in situ production as a key source of labile organic matter in hadal surface sediment of the Atacama Trench. Biogeosciences **19**: 1395–1420. doi:10.5194/bg-19-1395-2022

Follett, C. L., D. J. Repeta, D. H. Rothman, L. Xu, and C. Santinelli. 2014. Hidden cycle of dissolved organic carbon in the deep ocean. Proc. Natl. Acad. Sci. U.S.A. **111**: 16706–16711. doi:10.1073/pnas.1407445111

García-Martín, E. E., M. Aranguren-Gassis, D. M. Karl, S. Martínez-García, C. Robinson, P. Serret, and E. Teira. 2019. Validation of the in vivo Iodo-Nitro-Tetrazolium (INT) salt reduction method as a proxy for plankton respiration. Front. Mar. Sci. **6**: 220. doi:10.3389/fmars.2019.00220

Gloege, L., G. A. McKinley, C. B. Mouw, and A. B. Ciochetto. 2017. Global evaluation of particulate organic carbon flux parameterizations and implications for atmospheric pCO_2. Glob. Biogeochem. Cycl. **31**: 1192–1215. doi:10.1002/2016gb005535

Glud, R. N., and others. 2021. Hadal trenches are dynamic hotspots for early diagenesis in the deep sea. Commun. Earth Environ. **2**: 21. doi:10.1038/s43247-020-00087-2

Glud, R. N., F. Wenzhofer, M. Middelboe, K. Oguri, R. Turnewitsch, D. E. Canfield, and H. Kitazato. 2013. High rates of microbial carbon turnover in sediments in the deepest oceanic trench on Earth. Nat. Geosci. **6**: 284–288. doi:10.1038/ngeo1773

González, H. E., and others. 2009. Carbon fluxes within the epipelagic zone of the Humboldt Current System off Chile: The significance of euphausiids and diatoms as key functional groups for the biological pump. Prog. Oceanogr. **83**: 217–227. doi:10.1016/j.pocean.2009.07.036

Griffith, D. R., A. P. McNichol, L. Xu, F. A. McLaughlin, R. W. Macdonald, K. A. Brown, and T. I. Eglinton. 2012. Carbon dynamics in the western Arctic Ocean: insights from full-depth carbon isotope profiles of DIC, DOC, and POC. Biogeosciences **9**: 1217–1224. doi:10.5194/bg-9-1217-2012

Guerrero-Feijóo, E., E. Sintes, G. J. Herndl, and M. M. Varela. 2018. High dark inorganic carbon fixation rates by specific microbial groups in the Atlantic off the Galician coast (NW Iberian margin). Environ. Microbiol. **20**: 602–611. doi:10.1111/1462-2920.13984

Guidi, L., L. Legendre, G. Reygondeau, J. Uitz, L. Stemmann, and S. A. Henson. 2015. A new look at ocean carbon remineralization for estimating deepwater sequestration. Glob. Biogeochem. Cycl. **29**: 1044–1059. doi:10.1002/2014GB005063

Hama, T., T. Miyazaki, Y. Ogawa, T. Iwakuma, M. Takahashi, A. Otsuki, and S. Ichimura. 1983. Measurement of

photosynthetic production of a marine phytoplankton population using a stable ^{13}C isotope. Mar. Biol. **73**: 31–36. doi:10.1007/BF00396282

Henson, S. A., R. Sanders, and E. Madsen. 2012. Global patterns in efficiency of particulate organic carbon export and transfer to the deep ocean. Glob. Biogeochem. Cycl. **26**: GB1028. doi:10.1029/2011GB004099

Herndl, G. J., and T. Reinthaler. 2013. Microbial control of the dark end of the biological pump. Nat. Geosci. **6**: 718–724. doi:10.1038/ngeo1921

Honda, M. C. 2020. Effective vertical transport of particulate organic carbon in the western North Pacific subarctic region. Front. Earth Sci. **8**: 366. doi:10.3389/feart.2020.00366

Ishiwatari, R., K. Yamada, K. Matsumoto, H. Naraoka, S. Yamamoto, and N. Handa. 2000. Source of organic matter in sinking particles in the Japan Trench: Molecular composition and carbon isotopic analyses, p. 141–168. *In* N. Handa, E. Tanoue, and T. Hama [eds.], Dynamics and characterization of marine organic matter. Springer Netherlands.

Jamieson, A. J. 2015. The hadal zone: Life in the deepest oceans. Cambridge University Press.

Jamieson, A. J., T. Fujii, D. J. Mayor, M. Solan, and I. G. Priede. 2010. Hadal trenches: The ecology of the deepest places on Earth. Trends Ecol. Evol. **25**: 190–197. doi:10.1016/j.tree.2009.09.009

Kwak, J. H., S. H. Lee, H. J. Park, E. J. Choy, H. D. Jeong, K. R. Kim, and C. K. Kang. 2013. Monthly measured primary and new productivities in the Ulleung Basin as a biological "hot spot" in the East/Japan Sea. Biogeosciences **10**: 4405–4417. doi:10.5194/bg-10-4405-2013

Lengger, S. K., and others. 2019. Dark carbon fixation in the Arabian Sea oxygen minimum zone contributes to sedimentary organic carbon (SOM). Glob. Biogeochem. Cycl. **33**: 1715–1732. doi:10.1029/2019GB006282

Liu, J., and others. 2019. Proliferation of hydrocarbon-degrading microbes at the bottom of the Mariana Trench. Microbiome **7**: 47. doi:10.1186/s40168-019-0652-3

Lovecchio, E., N. Gruber, M. Münnich, and Z. Lachkar. 2017. On the long-range offshore transport of organic carbon from the Canary Upwelling System to the open North Atlantic. Biogeosciences **14**: 3337–3369. doi:10.5194/bg-14-3337-2017

Martin, J. H., G. A. Knauer, D. M. Karl, and W. W. Broenkow. 1987. VERTEX: Carbon cycling in the northeast Pacific. Deep Sea Res. A Oceanogr. Res. Pap. **34**: 267–285. doi:10.1016/0198-0149(87)90086-0

Martinez-Garcia, S., E. Fernandez, M. Aranguren-Gassis, and E. Teira. 2009. In vivo electron transport system activity: A method to estimate respiration in natural marine microbial planktonic communities. Limnol. Oceanogr. Methods **7**: 459–469. doi:10.4319/lom.2009.7.459

Martinez-Garcia, S., and others. 2018. Control of net community production by microbial community respiration at

Station ALOHA. J. Mar. Syst. **184**: 28–35. doi:10.1016/j.jmarsys.2018.03.007

Middelburg, J. J. 2011. Chemoautotrophy in the ocean. Geophys. Res. Lett. **38**: L24604. doi:10.1029/2011GL049725

Minutoli, R., and L. Guglielmo. 2009. Zooplankton respiratory Electron Transport System (ETS) activity in the Mediterranean Sea: Spatial and diel variability. Mar. Ecol. Prog. Ser. **381**: 199–211. doi:10.3354/meps07862

Molari, M., E. Manini, and A. Dell'Anno. 2013. Dark inorganic carbon fixation sustains the functioning of benthic deep-sea ecosystems. Glob. Biogeochem. Cycl. **27**: 212–221. doi:10.1002/gbc.20030

Morgan, J. P., and C. R. Ranero. 2023. Chapter 21—Roles of serpentinization in plate tectonics and the evolution of earth's mantle, p. 511–537. *In* J. C. Duarte [ed.], Dynamics of plate tectonics and mantle convection. Elsevier. doi:10.1016/B978-0-323-85733-8.00011-1

Mousseau, L., S. Dauchez, L. Legendre, and L. Fortier. 1995. Photosynthetic carbon uptake by marine phytoplankton: Comparison of the stable (^{13}C) and radioactive (^{14}C) isotope methods. J. Plankton Res. **17**: 1449–1460. doi:10.1093/plankt/17.7.1449

Nagata, T., and others. 2010. Emerging concepts on microbial processes in the bathypelagic ocean-ecology, biogeochemistry, and genomics. Deep-Sea Res. II Top. Stud. Oceanogr. **57**: 1519–1536. doi:10.1016/j.dsr2.2010.02.019

Nunoura, T., and others. 2015. Hadal biosphere: insight into the microbial ecosystem in the deepest ocean on Earth. Proc. Natl. Acad. Sci. U.S.A. **112**: E1230–E1236. doi:10.1073/pnas.1421816112

Nunoura, T., and others. 2016. Distribution and niche separation of planktonic microbial communities in the water columns from the surface to the hadal waters of the Japan Trench under the Eutrophic Ocean. Front. Microbiol. **7**: 1261. doi:10.3389/fmicb.2016.01261

Packard, T. T., N. Osma, I. Fernández-Urruzola, L. A. Codispoti, J. P. Christensen, and M. Gómez. 2015. Peruvian upwelling plankton respiration: calculations of carbon flux, nutrient retention efficiency, and heterotrophic energy production. Biogeosciences **12**: 2641–2654. doi:10.5194/bg-12-2641-2015

Paull, C. K., and others. 2018. Powerful turbidity currents driven by dense basal layers. Nat. Commun. **9**: 4114. doi:10.1038/s41467-018-06254-6

Ranero, C. R., J. Phipps Morgan, K. McIntosh, and C. Reichert. 2003. Bending-related faulting and mantle serpentinization at the Middle America trench. Nature **425**: 367–373. doi:10.1038/nature01961

Reinthaler, T., and others. 2006. Prokaryotic respiration and production in the meso- and bathypelagic realm of the eastern and western North Atlantic basin. Limnol. Oceanogr. **51**: 1262–1273. doi:10.4319/lo.2006.51.3.1262

Schrope, M. 2014. Journey to the bottom of the sea. Sci. Am. **310**: 60–69. doi:10.1038/scientificamerican0414-60

Shen, J., and others. 2020. Laterally transported particles from margins serve as a major carbon and energy source for dark ocean ecosystems. Geophys. Res. Lett. **47**: e2020GL088971. doi:10.1029/2020gl088971

Sigman, D. M., and M. P. Hain. 2012. The biological productivity of the ocean. Nat. Educ. Knowl. **3**: 21.

Sippl, C., B. Schurr, G. Asch, and J. Kummerow. 2018. Seismicity structure of the northern Chile forearc from >100,000 double-difference relocated hypocenters. J. Geophys. Res. Solid Earth **123**: 4063–4087. doi:10.1002/2017jb015384

Stief, P., M. Elvert, and R. N. Glud. 2021. Respiration by "marine snow" at high hydrostatic pressure: Insights from continuous oxygen measurements in a rotating pressure tank. Limnol. Oceanogr. **66**: 2797–2809. doi:10.1002/lno.11791

Tarn, J., L. M. Peoples, K. Hardy, J. Cameron, and D. H. Bartlett. 2016. Identification of free-living and particle-associated microbial communities present in hadal regions of the Mariana Trench. Front. Microbiol. **7**: 665. doi:10.3389/fmicb.2016.00665

Thijs, S., and others. 2017. Comparative evaluation of four bacteria-specific primer pairs for 16S rRNA gene surveys. Front. Microbiol. **8**: 494. doi:10.3389/fmicb.2017.00494

Tian, J., and others. 2018. A nearly uniform distributional pattern of heterotrophic bacteria in the Mariana Trench interior. Deep-Sea Res. I Oceanogr. Res. Pap. **142**: 116–126. doi:10.1016/j.dsr.2018.10.002

Turner, J. T. 2015. Review: Zooplankton fecal pellets, marine snow, phytodetritus and the ocean's biological pump. Prog. Oceanogr. **130**: 205–248. doi:10.1016/j.pocean.2014.08.005

Turnewitsch, R., and others. 2014. Recent sediment dynamics in hadal trenches: Evidence for the influence of higher-frequency (tidal, near-inertial) fluid dynamics. Deep Sea Res. **90**: 125–138. doi:10.1016/j.dsr.2014.05.005

Villegas-Mendoza, J., R. Cajal-Medrano, and H. Maske. 2019. The chemical transformation of the cellular toxin INT (2-(4-iodophenyl)-3-(4-nitrophenyl)-5-(phenyl) tetrazolium chloride) as an indicator of prior respiratory activity in aquatic bacteria. Int. J. Mol. Sci. **20**: 782. doi:10.3390/ijms20030782

Xu, Y., and others. 2021. Distribution, source, and burial of sedimentary organic carbon in Kermadec and Atacama Trenches. J. Geophys. Res. Biogeosci. **126**: e2020JG006189. doi:10.1029/2020JG006189

Zhou, W., J. Liao, Y. Guo, X. Yuan, H. Huang, T. Yuan, and S. Liu. 2017. High dark carbon fixation in the tropical South China Sea. Cont. Shelf Res. **146**: 82–88. doi:10.1016/j.csr.2017.08.005

Acknowledgments

Conflict of Interest Statement

The authors declare no conflict of interest.